
You Do Not Fully Utilize Transformer’s Representation Capacity

Gleb Gerasimov^{1,2,3†}

Yaroslav Aksenov^{1† *}

Nikita Balagansky^{1,2}

Viacheslav Sini¹

Daniil Gavrilov¹

[†]Equal contribution ¹T-Tech ²Moscow Institute of Physics and Technology ³HSE University

Abstract

In contrast to RNNs, which compress their history into a single hidden state, Transformers can attend to all past tokens directly. However, standard Transformers rely solely on the hidden state from the previous layer to represent the entire context. We show that this design choice induces representation collapse and degrades performance. To address this issue, we introduce *Layer-Integrated Memory* (LIMe), a lightweight extension that leverages existing key–value buffers and learns per-head, per-layer routing weights to integrate representations from all previous layers with negligible overhead. Through extensive experiments—including language modeling, synthetic reasoning benchmarks, and very deep architectures—LIMe consistently achieves faster convergence, lower perplexity per FLOP, and substantial accuracy improvements on synthetic tasks while preserving higher value–vector entropy and improved token separability. Finally, our analysis of the learned routing weights reveals systematic reuse of both local and long-distance features, demonstrating how LIMe mitigates collapse, unlocks richer representations without increasing hidden-state size, and points to promising directions for future research.

1 Introduction

Transformers [Vaswani et al., 2017] have become a central architecture in modern machine learning, powering state-of-the-art solutions in language modeling, computer vision, and beyond. Their ability to capture complex patterns arises from deeply stacked layers that refine contextual representations. However, despite their success, standard Transformer decoders maintain a single residual stream per layer, forcing the model to compress all previously learned features into the immediately preceding hidden state [Srivastava et al., 2015, He et al., 2015]. This design choice can lead to *representation collapse*—a phenomenon in which different tokens or features become indistinguishable in deeper layers [Voita et al., 2019, Barbero et al., 2024, Arefin et al., 2024]. The problem is particularly pronounced when learning from lengthy sequences, where subtle token distinctions risk being squeezed out by limited floating-point precision and finite hidden-state capacity.

In this paper, we propose *Layer-Integrated Memory* (**LIMe**)², a lightweight extension to multi-head self-attention that enables each attention head to retrieve and integrate representations from all

*Corresponding author: y.o.aksenov@tbank.ru

²Code available at <https://github.com/corl-team/lime>

preceding layers—rather than relying solely on the most recent hidden state. LIMe accomplishes this by learning a per-layer, per-head routing mechanism that efficiently blends multi-layer Key–Value features, all while preserving the core Transformer structure and adding negligible overhead by reusing already allocated Key–Value buffers.

Our key contributions are:

- **Layer-Integrated Routing.** A trainable router that, for each head at every layer, dynamically weights and mixes buffered Key–Value representations from all earlier layers, without increasing hidden-state dimensions or memory footprint.
- **Strong Empirical Gains.** LIMe converges 15.3% (8.9% with GQA) faster in FLOPs and achieves 1.15% (0.91% with GQA) lower perplexity than 1B-parameter LLaMa-based [Grattafiori et al., 2024] transformer, yields up to +8% on ProsQA [Hao et al., 2024] and +30% on arithmetic reasoning benchmarks [Arefin et al., 2024, Feng et al., 2023]. In deep settings (32, 64, 128 layers), a 64-layer LIMe matches a 128-layer baseline, indicating superior scaling behavior.
- **Mitigating Collapse.** An empirical analysis showing that LIMe preserves higher Rényi entropy [Arefin et al., 2024] and better token separability [Voita et al., 2019] in value spaces, effectively alleviating representation collapse.

Together, these results confirm that by distributing representational burden across persistent Key–Value buffers and learning to route information across layers, LIMe substantially improves both optimization efficiency and representational capacity, especially in tasks requiring long-range or multi-step reasoning, opening the door of utilizing LIMe for cutting-edge area of latent-space reasoning.

2 Related Work

Early works on training very deep networks highlighted the need for mechanisms to ease gradient flow and information propagation. Highway Networks introduce gated skip connections to regulate information flow across layers [Srivastava et al., 2015]. Deep Residual Networks further simplify this by adding identity shortcuts, enabling networks to exceed a hundred layers without suffering from vanishing gradients [He et al., 2015]. Transformers adopt a similar residual-plus-normalization design, which underpins their success in language and vision tasks [Vaswani et al., 2017, Grattafiori et al., 2024, Jiang et al., 2023, Qwen et al., 2024, DeepSeek-AI et al., 2024].

Although residual streams facilitate training, they still force each layer to compress all prior features into a single vector, which can lead to *representation collapse*—distinct inputs becoming indistinguishable in deeper layers. Tenney et al. [2019] found that BERT’s deeper layers refine earlier predictions using higher-level context. Voita et al. [2019] empirically demonstrated that Transformers’ top layers lose fine-grained token distinctions. Theoretically, Barbero et al. [2024] proved that decoder-only Transformers can exhibit arbitrarily close final-token representations for different inputs, a phenomenon akin to *over-squashing*. Building on this, Hahn and Rofin [2024] showed that the loss landscape of Transformers biases them toward low-sensitivity functions, exacerbating collapse. Recently, Arefin et al. [2024] introduced Seq-VCR, a variance–covariance regularizer that preserves intermediate representation diversity and significantly improves multi-step reasoning performance.

To mitigate collapse, several works have explored aggregating information across layers. Cross-Layer Retrospective Retrieving learns dynamic attention weights over prior layer outputs for each head [Fang et al., 2023]. Hyper-Connections augment Transformers with multiple residual streams that interact via learned projections, preventing collapse at the cost of increased hidden-state size [Zhu et al., 2024]. Although Mixture-of-Depths [Raposo et al., 2024] focuses on reducing FLOPs by skipping token computations layer-wise, its dynamic routing approach resonates with our per-head, per-layer routing mechanism; unlike MoD, LIMe retains full dense computation while enriching representational capacity through routing over pre-allocated key–value buffers. Different architectures based on usage of previous representations were proposed in [Huang et al., 2018, Bapna et al., 2018, Wu et al., 2023]. Despite these advances, most methods require substantial architectural changes or extra memory. Our method, Layer-Integrated Memory (LIMe), instead *reuses* existing key–value buffers and learns per-head, per-layer routing to mix multi-layer representations with negligible memory and speed overhead (see Appendix F).



Figure 1: Training loss per FLOPs for LLaMa and LIME. LIME has a substantially lower loss with a similar amount of FLOPs. See Section 5.1 for more details.

3 Preliminaries

Notation. Let t denote the sequence length (temporal dimension), d the model dimension, H the number of attention heads, $d_{\text{head}} = d/H$ the dimension of each head, and L the total number of layers. We denote by $\mathbf{X}_{\ell-1} \in \mathbb{R}^{t \times d}$ the residual stream entering layer ℓ , with $\ell = 1, \dots, L$.

Causal Self-Attention. Let

$$\mathbf{Q} = \mathbf{X} \mathbf{W}^{(Q)}, \quad \mathbf{K} = \mathbf{X} \mathbf{W}^{(K)}, \quad \mathbf{V} = \mathbf{X} \mathbf{W}^{(V)},$$

with $\mathbf{W}^{(Q)}, \mathbf{W}^{(K)}, \mathbf{W}^{(V)} \in \mathbb{R}^{d \times d}$. Splitting into H heads of dimension $d_h = d/H$ yields $\{\mathbf{Q}_i, \mathbf{K}_i, \mathbf{V}_i\}_{i=1}^H$. For head i ,

$$\text{head}_i = \text{softmax}\left(\frac{\mathbf{Q}_i \mathbf{K}_i^\top}{\sqrt{d_h}} + \mathbf{M}\right) \mathbf{V}_i \in \mathbb{R}^{t \times d_h},$$

where \mathbf{M} masks future positions. The heads are concatenated across the last dimension and projected:

$$\text{MultiHeadAttn}(\mathbf{X}) = \text{Concat}(\text{head}_1, \dots, \text{head}_H) \mathbf{W}^{(O)}, \quad \mathbf{W}^{(O)} \in \mathbb{R}^{d \times d}.$$

Residual connections. Denoting a sub-layer function $\mathcal{F}(\cdot)$ and input \mathbf{X} , the pre-norm residual update is

$$\mathbf{X}' = \mathbf{X} + \mathcal{F}(\text{RMSNorm}(\mathbf{X})).$$

4 Method

We introduce *Layer-Integrated Memory* (LIME), a lightweight mechanism to augment a decoder-only Transformer with inter-layer, learnable information flow. Unlike standard multi-head attention (MHA), which attends only to the current layer’s residual stream, LIME enables each head to retrieve and fuse Key–Value representations from all earlier layers. This enriches the model’s representation capacity without increasing memory use, since we reuse the Key–Value buffers already allocated by vanilla Transformers.

At a high level, each LIME attention layer performs three steps:

1. Compute and *buffer* per-head Key–Value projections from the current residual stream.
2. *Route* by forming a learned mixture of all buffered Key and Value heads’ states up to the current layer.
3. Compute attention between the current layer’s Queries and the routed Key–Value mixture.

Visualisation of the architecture can be found in Appendix G.

1. Key–Value Buffering. At layer ℓ , we compute per-head Key and Value tensors in the usual way:

$$\mathbf{K}_\ell = \mathbf{X}_{\ell-1} W_\ell^{(K)}, \quad \mathbf{V}_\ell = \mathbf{X}_{\ell-1} W_\ell^{(V)}, \quad \mathbf{K}_\ell, \mathbf{V}_\ell \in \mathbb{R}^{t \times H \times d_h}. \quad (1)$$

We then store these in the pre-allocated buffers

$$\mathcal{B}^{(K)}, \mathcal{B}^{(V)} \in \mathbb{R}^{L \times H \times t \times d_h},$$

for Keys and Values respectively. No extra memory is required, since vanilla Transformers already maintain all per-layer Key–Value states for training and cache them during inference for generation efficiency. See Appendix F for details.

2. Inter-Layer Routing. To enable each head at layer ℓ to *mix* information from all previous layers, we introduce a trainable router tensor $R^{(\ell)} \in \mathbb{R}^{\ell \times H \times H}$, where $R_{\ell',h',h}^{(\ell)}$ is a weight from head h' at layer ℓ' into head h at layer ℓ .

Using buffer we route keys and values for each head h :

$$\tilde{\mathbf{K}}_{\ell,h} = \sum_{\ell'=1}^{\ell} \sum_{h'=1}^H R_{\ell',h',h}^{(\ell)} \mathcal{B}_{\ell',h'}^{(K)}, \quad \text{and} \quad \tilde{\mathbf{V}}_{\ell,h} = \sum_{\ell'=1}^{\ell} \sum_{h'=1}^H R_{\ell',h',h}^{(\ell)} \mathcal{B}_{\ell',h'}^{(V)}. \quad (2)$$

3. Attention with Layer-Integrated Memory. We compute the usual per-head Queries,

$$\mathbf{Q}_{\ell,h} = \mathbf{X}_{\ell-1} W_{\ell,h}^{(Q)}, \quad \mathbf{Q}_{\ell,h} \in \mathbb{R}^{t \times d_h},$$

and then perform scaled dot-product attention for each head between $\mathbf{Q}_{\ell,h}$ and the routed $\tilde{\mathbf{K}}_{\ell,h}, \tilde{\mathbf{V}}_{\ell,h}$.

LIMe Advantages. By routing through all prior layers, LIMe endows each head with a learnable, layer-wise memory. Unlike fixed skip connections or naive averaging, LIMe learns per-head, per-layer weightings, enabling selective retrieval and *forgetting* of past representations. Despite this added flexibility, the extra computation is only linear in sequence length. Crucially, LIMe is fully compatible with efficient MHA implementations such as FlashAttention [Dao, 2024], and it introduces negligible additional memory footprint by reusing existing Key–Value buffers (see Appendix F for details). In Appendix D, we include an ablation study on restricted router weights, demonstrating the importance of the trained router in LIMe.

5 Experiments

5.1 Language Modeling

We evaluate the effectiveness of **LIMe** against two baselines: **LLaMa** [Grattafiori et al., 2024] and **Hyper Connections** [Zhu et al., 2024]. All models have approximately 1B parameters and share the same underlying transformer architecture (see Table 3). We trained each model from scratch on the *FineWeb Edu* [Penedo et al., 2024] subset with about 50B tokens. The full training setup can be found in Appendix A.

Figure 1 displays the iso-flops training loss curves, demonstrating that LIMe converges more rapidly and achieves lower perplexities than LLaMa, indicating improved parameter efficiency. Details on model efficiency and FLOPs calculations can be found in Appendix F. Table 1 presents results on the 3-shot LM Eval Harness benchmarks Wang et al. [2018, 2019], Srivastava et al. [2023], further highlighting the advantages conferred by LIMe on language modeling over baseline models. For more benchmarks see Appendix C. In the next section, we go deeper into the factors driving these gains.

5.2 Measuring Representation Collapse

Recent work has shown that large language models (LLMs) can suffer from *representation collapse* when representing long sequences, thereby forcing subtle token distinctions to become inseparable in deeper layers [Voita et al., 2019, Arefin et al., 2024]. We investigate this phenomenon by comparing LLaMa [Grattafiori et al., 2024] and LIMe via two complementary approaches: (i) quantifying

Model	MultiRC	WiC	QNLI	ARC-E	ARC-C	KV	Induction	LD-3	Avg
LLaMA	43.24	50.00	49.49	70.45	38.70	45.94	54.20	33.60	48.20
HC	54.34	49.72	49.43	71.15	37.63	51.68	51.59	33.87	49.93
LIME	56.15	50.44	51.43	71.15	39.30	55.64	55.36	34.47	51.74

Table 1: LM Evaluation Harness benchmarks results on 1B models with GQA in 3-shot setup. LIME outperforms both LLaMA and Hyper-Connections baselines. See details in Section 5.1.

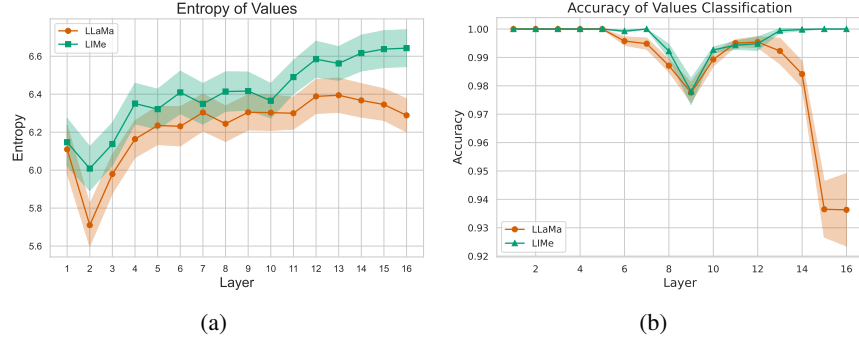


Figure 2: (a) Matrix entropy of values on the FineWeb Edu subset by layer. LIME has more diverse values than LLaMA, which indicates that more information is stored in its hidden states. (b) Values’ classification accuracy, with standard deviation over five cross-validation folds. Values in later layers obtained from LIME can be linearly separated with nearly 1.0 accuracy, whereas the accuracy for values from LLaMA is much lower. See Section 5.2 for more details.

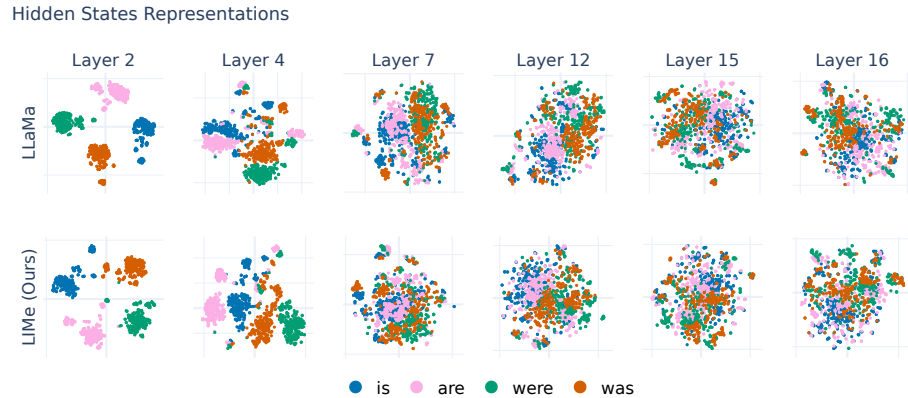
the diversity of hidden states and values with *matrix-based Rényi entropy* [Arefin et al., 2024] and (ii) measuring and visualizing the linear separability of layer-wise embeddings of closely related tokens (is, are, was, were) [Voita et al., 2019]. These two methodologies directly measure representation collapse in language models.

Unlike Arefin et al. [2024], we evaluate both residual-stream hidden states and value representations. We expect weaker linear separability in hidden states (because the model need not pack all information there) and stronger separation in value vectors. For matrix entropy, we anticipate little change at the hidden-state level but a clear difference for value representations. At each layer ℓ , we record *value states* (i.e., the output of the $W_\ell^{(V)}$ linear projection) and *hidden states* (i.e., the residual stream \mathbf{X}_ℓ).

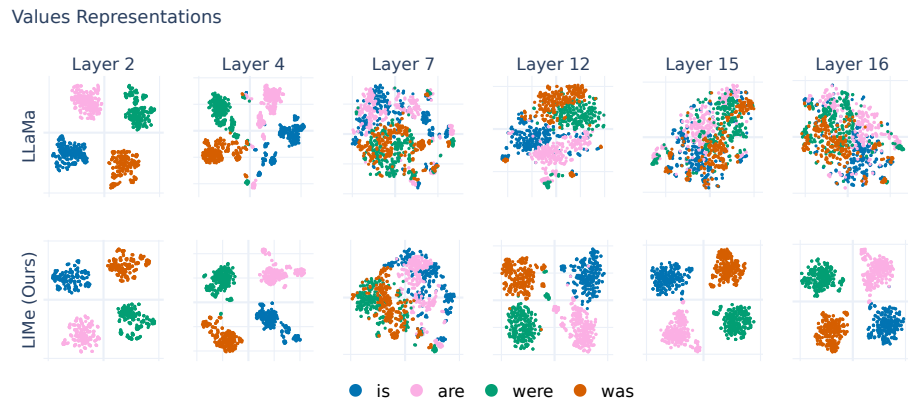
Matrix-Based Rényi Entropy. Following Arefin et al. [2024], we measure the diversity of representations at layer ℓ by forming the Gram matrix $\mathbf{K} = Z^{(\ell)} Z^{(\ell)\top} \in \mathbb{R}^{t \times t}$, where $Z^{(\ell)}$ contains the d -dimensional representations of t tokens. Let $\{\lambda_i(\mathbf{K})\}_{i=1}^t$ be the eigenvalues of \mathbf{K} . We define the α -order Rényi entropy as $S_\alpha(Z^{(\ell)}) = \frac{1}{1-\alpha} \log \left[\sum_{i=1}^t \left(\frac{\lambda_i(\mathbf{K})}{\text{tr}(\mathbf{K})} \right)^\alpha \right]$. Each eigenvalue is normalized by $\text{tr}(\mathbf{K})$, ensuring the probabilities sum to 1. Higher S_α indicates greater variance (i.e., lower collapse).

Figure 2(a) shows that LIME yields significantly higher matrix entropy of gathered MHA values compared with LLaMA and shows no significant difference when evaluating hidden states (see Figure 7(a)).

Layer-Wise Token Separability. To more directly evaluate the level of representation collapse, we replicate the methodology of Voita et al. [2019], extracting 1668 occurrences each of is, are, was, were from the *FineWeb Edu* corpus. To quantify information collapse, we train a linear four-way classifier (for is, are, was, were) on layer-wise representations. Figure 2(b) shows mean classification accuracies (with five-fold cross-validation) for value representations layer by layer. We observe that LIME consistently exhibits higher classification accuracy than LLaMA, confirming that LIME’s value representations avoid collapse. As hypothesized, hidden states became less separable



(a)



(b)

Figure 3: (a) t-SNE of similar tokens’ hidden states among layers. Although hidden states are not separable in later layers for both models, unlike LLaMA, LIME can make updates attending to the previous representations, which leads to high values’ separability. (b) t-SNE of similar tokens’ values among layers shows higher separability for LIME’s representations. See Section 5.2 for more details.

for LIME, indicating that there was no need to store all necessary information in a single hidden state (see Figure 7(b)).

Additionally, we project representations into a two-dimensional space via t-SNE and visualize how well value states and hidden states can be clustered (Figure 3). In contrast to LIME, deeper-layer representations in LLaMA for such similar tokens often collapse into overlapping regions, reflecting the inclination of the vanilla transformer to heavily compress relevant information into a single representation and therefore blur small yet important differences.

Discussion. Together, these results corroborate our theoretical motivation: by allowing each head to attend directly to earlier-layer representations, LIME expands the overall representational capacity. This multi-layer routing reduces collapse in the *values* while freeing deeper *hidden* states from the burden of storing all lexical nuances—leading to higher overall entropy on values (Figure 2(a)) and improved model performance (Table 1). In the next section, we evaluate LIME on synthetic benchmarks where the model’s ability to store complex information in limited state capacity is crucial.

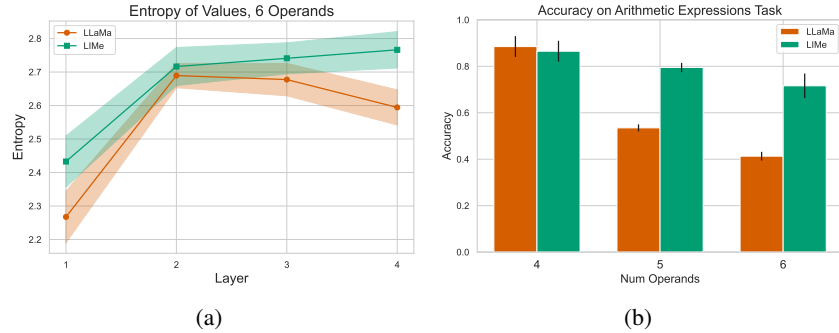


Figure 4: (a) LIME exhibits consistently higher entropy of value vectors across layers, particularly in the final layer, indicating reduced representation collapse compared to LLaMa. (b) On the Arithmetic Expressions task, LIME significantly outperforms the LLaMa baseline, maintaining high accuracy even as the number of operands increases, while LLaMa’s performance deteriorates. For details, see Section 5.3.2.

5.3 Evaluating Representation Collapse on Synthetic Tasks

5.3.1 Planning and Search Capabilities

We fine-tune models on ProsQA (Proof with Search Question-Answering) [Hao et al., 2024]. Each ProsQA instance presents a set of fictional concepts described via natural-language conditions arranged in a DAG, requiring models to determine the veracity of a target statement by exploring multiple reasoning paths over the graph (examples in Appendix B). Unlike linear chain-of-thought methods [Wei et al., 2022], ProsQA demands maintaining and evaluating parallel hypothesis streams akin to breadth-first search in latent reasoning [Hao et al., 2024]. In our experiments we evaluate both fine-tuned models on ProsQA task via open-ended reasoning generation. LLaMA achieves **69.4%** accuracy, meanwhile LIME achieves **77.8%** accuracy, outperforming LLaMA by **8.4%**. Since correct prediction requires searching over paths in the graph of input statements, baseline transformers suffer representation collapse from storing multiple reasoning chains in their hidden states, particularly for longer inference sequences. LIME mitigates this by distributing the reasoning process across layers — early layers may store primitive inferences while deeper layers compose them, maintaining better separation between similar reasoning paths.

5.3.2 Arithmetic Expression Benchmark

Standard one-shot QA benchmarks mainly test *final-token prediction*, which can often be solved via shallow pattern matching or retrieval, masking the role of intermediate representation quality in reasoning. To isolate the impact of multi-step computation, we adopt the Arithmetic Expression Task (AET) [Arefin et al., 2024, Feng et al., 2023], a synthetic benchmark presenting expressions over integer operands with operators $+$, $-$, \times , \div , along with solution steps and requiring the exact integer result. See examples in Appendix B.

Following Arefin et al. [2024], we generate 3 difficulty tiers comprising expressions with 4, 5, and 6 operands, accompanied by step-by-step solutions (details in Appendix A). While performing similarly to LLaMa on 4 operands, LIME achieves significantly higher accuracy after increasing number of operands to 5 and 6 (Figure 4(b)). LIME (**71.6%**) outperforms LLaMa (**41.3%**) by over **30%** in accuracy on 6 operands. These results go along with lower representation collapse which is illustrated by higher entropy of value representations shown in Figure 4(a). Also, LIME exhibits better separability of close numbers which leads to lower error rate in intermediate calculations, see Figure 8 in Appendix.

Arithmetic Expressions Task requires intermediate calculations to be performed correctly in order to get the correct final answer. The problem of representation collapse results in representations of close numbers being similar which leads to incorrect intermediate results, and thus the wrong final answer. Since LIME has access to previous representations at each layer, it preserves finer numerical distinctions in comparison with standard transformer architectures like LLaMa. Moreover, LIME has

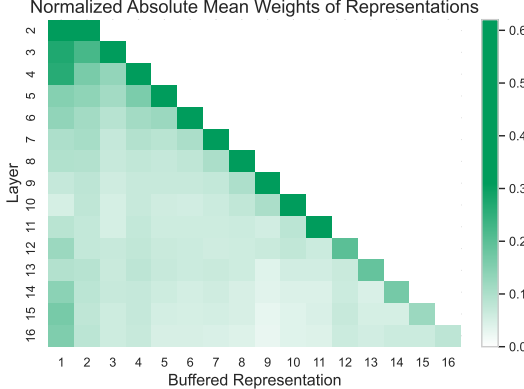


Figure 5: Mean retrieval weight for each buffered representation across subsequent layers. Larger diagonal values confirm reliance on the current residual stream, while the pronounced off-diagonal weights for the earliest buffers and the repeated reuse of intermediate ones show that the model systematically retrieves earlier features, providing auxiliary memory and helping to mitigate representation collapse. See Section 5.4 for more details.

ability to store information in earlier representations, i.e. performing computations at some early or intermediate layer, but using it further only in later layers, which also boosts its reasoning capabilities and leads to better results on tasks that require intermediate steps.

5.4 Analyzing Learned Routings in LIME

To understand *how* LIME routes information across layers and thereby mitigates representation collapse, we inspect the learned router weights. Since the router weights can be both positive and negative—and because random initialization of the key, value, and output projections renders their sign semantically ambiguous—we analyze the absolute magnitudes of these weights to quantify each buffered representation’s relative contribution in a sign-agnostic manner.

For each layer $\ell \geq 2$, we take the absolute magnitude of its router weights, average over heads for each buffered representation $j \leq \ell$, and then normalize these averages per layer. The resulting heatmap in Figure 5 shows the normalized mean weight: cell (ℓ, j) measures the average contribution of the keys and values generated at layer j to the attention computation in layer ℓ . In a standard Transformer without routing, each layer would attend solely to its own keys and values, yielding a heatmap with ones on the diagonal and zeros elsewhere; LIME departs markedly from this behavior.

Several clear patterns emerge:

- **Strong reliance on embeddings in early layers:** Layers 2-4 allocate much of their attention to the buffered representations from the embedding layer. This corroborates the view that the initial attention layers focus on capturing local and morphological relationships among tokens, and that LIME grants additional flexibility in reusing these low-level features.
- **Auxiliary memory via neighboring layers:** Early and middle layers place a share of attention on the buffered KV states of its immediate predecessor. This indicates that they can treat them as an auxiliary memory bank, effectively extending the subspace of features it can manipulate by leveraging projections made by other heads.
- **Long-distance retrieval from early buffers:** Higher layers also attend nontrivially to the first two buffered representations. The effect is especially pronounced in the final layers, suggesting that late-stage prediction benefits from revisiting the original token embeddings and shallow features.

By allowing flexible retrieval of features from arbitrarily distant layers, LIME relieves each residual stream from having to carry the entire contextual signal forward. Instead, information can be distributed across a set of persistent buffers, preserving a richer and more diverse feature set throughout the network’s depth and thereby mitigating representation collapse. For the full, detailed set of normalized router weights, see Appendix Figure 9.

5.5 Deep Networks Performance

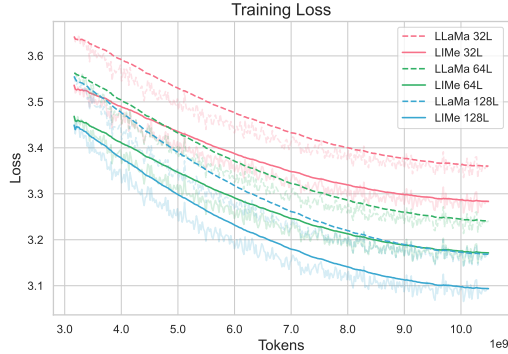


Figure 6: Training losses for deep architectures. The LIME models consistently outperform their LLaMA counterparts across all depths, with LIME with 64 layers outperforming LLaMA with 128 layers. See Section 5.5 for details.

Transformers scaled to increasing depths often suffer from representation collapse, which motivates our evaluation of LIME in 32-, 64-, and 128-layer configurations. We compare LIME against the baseline LLaMA, each using 8 attention heads per layer, and observe that LIME outperforms LLaMA at every tested depth (Fig. 6). Furthermore, LIME exhibits superior scaling behavior: as depth increases, its loss decreases more rapidly than LLaMA’s, implying that direct routing of earlier-layer features enhances the model’s effective representational capacity, whereas LLaMA’s single-stream residual architecture struggles to preserve fine-grained features across layers. Notably, a 64-layer LIME model outperforms a 128-layer LLaMA model, despite the latter requiring roughly twice the FLOPs and parameters. This suggests that the optimal scaling strategy for transformers may deviate from conventional practice, potentially favoring much deeper models with smaller hidden dimensions. We leave further investigation of these scaling dynamics to future work.

6 Conclusion and Future Work

In this paper, we proposed *Layer-Integrated Memory* (LIME), a lightweight extension to multi-head self-attention that enables each attention head to retrieve and integrate representations from all preceding layers. Through extensive experiments on language modeling, synthetic reasoning benchmarks, and deep transformer configurations, we demonstrated that LIME (i) accelerates convergence in FLOPs by up to 15.3% and reduces perplexity by up to 1.15% compared to standard Transformer decoders, yields improvements of up to +8% on the challenging ProsQA task and +30% on Arithmetic Reasoning Task; (ii) mitigates representation collapse by preserving higher entropy in value vectors and maintaining token separability in deeper layers; and (iii) enables shallower models to match or exceed the performance of double-sized deeper baselines. Our analysis of the learned routing weights further revealed that LIME systematically leverages both local and long-distance feature reuse, effectively distributing contextual information across layers without increasing the hidden-state size.

Limitations. While our method consistently yields better results on both benchmarks and language modeling tasks, it could lead to additional communication between GPUs in pipeline parallel setup. Also, vanilla implementation of the method has $\mathcal{O}(L^2)$ asymptotic, and some heuristics proposed in Appendix D might be useful for scaling.

Looking forward, two research directions emerge as particularly promising. First, a comprehensive exploration of the width-depth trade-off in LIME architectures could unveil optimal scaling regimes tailored to diverse tasks and computational budgets. Second, a rigorous theoretical analysis of the routing mechanism may inform principled designs for multi-layer memory, thereby enabling models to perform advanced latent-space reasoning grounded in Layer-Integrated Memory.

References

Quentin Anthony, Stella Biderman, and Hailey Schoelkopf. Transformer math 101. blog.eleuther.ai/, 2023. URL <https://blog.eleuther.ai/transformer-math/>.

Md Rifat Arefin, Gopesh Subbaraj, Nicolas Gontier, Yann LeCun, Irina Rish, Ravid Shwartz-Ziv, and Christopher Pal. Seq-vcr: Preventing collapse in intermediate transformer representations for enhanced reasoning. *arXiv preprint arXiv: 2411.02344*, 2024.

Ankur Bapna, Mia Chen, Orhan Firat, Yuan Cao, and Yonghui Wu. Training deeper neural machine translation models with transparent attention. In *Proceedings of the 2018 Conference on Empirical Methods in Natural Language Processing (EMNLP)*, pages 3028–3033, 2018. doi: 10.18653/v1/D18-1338. URL <https://arxiv.org/abs/1808.07561>. arXiv:1808.07561.

Federico Barbero, Andrea Banino, Steven Kapturowski, Dharshan Kumaran, João G. M. Araújo, Alex Vitvitskyi, Razvan Pascanu, and Petar Velicković. Transformers need glasses! information over-squashing in language tasks. *arXiv preprint arXiv: 2406.04267*, 2024.

Tri Dao. FlashAttention-2: Faster attention with better parallelism and work partitioning. In *International Conference on Learning Representations (ICLR)*, 2024.

DeepSeek-AI, Aixin Liu, Bei Feng, Bin Wang, Bingxuan Wang, Bo Liu, Chenggang Zhao, Chengqi Dengr, Chong Ruan, Damai Dai, Daya Guo, Dejian Yang, Deli Chen, Dongjie Ji, Erhang Li, Fangyun Lin, Fuli Luo, Guangbo Hao, Guanting Chen, Guowei Li, H. Zhang, Hanwei Xu, Hao Yang, Haowei Zhang, Honghui Ding, Huajian Xin, Huazuo Gao, Hui Li, Hui Qu, J. L. Cai, Jian Liang, Jianzhong Guo, Jiaqi Ni, Jiaoshi Li, Jin Chen, Jingyang Yuan, Junjie Qiu, Junxiao Song, Kai Dong, Kaige Gao, Kang Guan, Lean Wang, Lecong Zhang, Lei Xu, Leyi Xia, Liang Zhao, Liyue Zhang, Meng Li, Miaojun Wang, Mingchuan Zhang, Minghua Zhang, Minghui Tang, Mingming Li, Ning Tian, Panpan Huang, Peiyi Wang, Peng Zhang, Qihao Zhu, Qinyu Chen, Qiushi Du, R. J. Chen, R. L. Jin, Ruiqi Ge, Ruizhe Pan, Runxin Xu, Ruyi Chen, S. S. Li, Shanghao Lu, Shangyan Zhou, Shanhua Chen, Shaoqing Wu, Shengfeng Ye, Shirong Ma, Shiyu Wang, Shuang Zhou, Shuiping Yu, Shunfeng Zhou, Size Zheng, T. Wang, Tian Pei, Tian Yuan, Tianyu Sun, W. L. Xiao, Wangding Zeng, Wei An, Wen Liu, Wenfeng Liang, Wenjun Gao, Wentao Zhang, X. Q. Li, Xiangyue Jin, Xianzu Wang, Xiao Bi, Xiaodong Liu, Xiaohan Wang, Xiaojin Shen, Xiaokang Chen, Xiaosha Chen, Xiaotao Nie, Xiaowen Sun, Xiaoxiang Wang, Xin Liu, Xin Xie, Xingkai Yu, Xinnan Song, Xinyi Zhou, Xinyu Yang, Xuan Lu, Xuecheng Su, Y. Wu, Y. K. Li, Y. X. Wei, Y. X. Zhu, Yanhong Xu, Yanping Huang, Yao Li, Yao Zhao, Yaofeng Sun, Yaohui Li, Yaohui Wang, Yi Zheng, Yichao Zhang, Yiliang Xiong, Yilong Zhao, Ying He, Ying Tang, Yishi Piao, Yixin Dong, Yixuan Tan, Yiyuan Liu, Yongji Wang, Yongqiang Guo, Yuchen Zhu, Yuduan Wang, Yuheng Zou, Yukun Zha, Yunxian Ma, Yuting Yan, Yuxiang You, Yuxuan Liu, Z. Z. Ren, Zehui Ren, Zhangli Sha, Zhe Fu, Zhen Huang, Zhen Zhang, Zhenda Xie, Zhewen Hao, Zhihong Shao, Zhiniu Wen, Zhipeng Xu, Zhongyu Zhang, Zhuoshu Li, Zihan Wang, Zihui Gu, Zilin Li, and Ziwei Xie. Deepseek-v2: A strong, economical, and efficient mixture-of-experts language model. *arXiv preprint arXiv: 2405.04434*, 2024.

Yanwen Fang, Yuxi Cai, Jintai Chen, Jingyu Zhao, Guangjian Tian, and Guodong Li. Cross-layer retrospective retrieving via layer attention. In *The Eleventh International Conference on Learning Representations, ICLR 2023, Kigali, Rwanda, May 1-5, 2023*. OpenReview.net, 2023. URL <https://openreview.net/forum?id=pvgEL1yS3Q1>.

Guahao Feng, Bohang Zhang, Yuntian Gu, Haotian Ye, Di He, and Liwei Wang. Towards revealing the mystery behind chain of thought: A theoretical perspective, 2023. URL <https://arxiv.org/abs/2305.15408>.

Aaron Grattafiori, Abhimanyu Dubey, Abhinav Jauhri, Abhinav Pandey, Abhishek Kadian, Ahmad Al-Dahle, Aiesha Letman, Akhil Mathur, Alan Schelten, Alex Vaughan, Amy Yang, Angela Fan, Anirudh Goyal, Anthony Hartshorn, Aobo Yang, Archi Mitra, Archie Sravankumar, Artem Korenev, Arthur Hinsvark, Arun Rao, Aston Zhang, Aurelien Rodriguez, Austen Gregerson, Ava Spataru, Baptiste Roziere, Bethany Biron, Binh Tang, Bobbie Chern, Charlotte Caucheteux, Chaya Nayak, Chloe Bi, Chris Marra, Chris McConnell, Christian Keller, Christophe Touret, Chunyang Wu, Corinne Wong, Cristian Canton Ferrer, Cyrus Nikolaidis, Damien Allonsius, Daniel Song, Danielle Pintz, Danny Livshits, Danny Wyatt, David Esiobu, Dhruv Choudhary, Dhruv Mahajan,

Diego Garcia-Olano, Diego Perino, Dieuwke Hupkes, Egor Lakomkin, Ehab AlBadawy, Elina Lobanova, Emily Dinan, Eric Michael Smith, Filip Radenovic, Francisco Guzmán, Frank Zhang, Gabriel Synnaeve, Gabrielle Lee, Georgia Lewis Anderson, Govind Thattai, Graeme Nail, Gregoire Mialon, Guan Pang, Guillem Cucurell, Hailey Nguyen, Hannah Korevaar, Hu Xu, Hugo Touvron, Iliyan Zarov, Imanol Arrieta Ibarra, Isabel Kloumann, Ishan Misra, Ivan Evtimov, Jack Zhang, Jade Copet, Jaewon Lee, Jan Geffert, Jana Vranes, Jason Park, Jay Mahadeokar, Jeet Shah, Jelmer van der Linde, Jennifer Billock, Jenny Hong, Jenya Lee, Jeremy Fu, Jianfeng Chi, Jianyu Huang, Jiawen Liu, Jie Wang, Jiecao Yu, Joanna Bitton, Joe Spisak, Jongsoo Park, Joseph Rocca, Joshua Johnstun, Joshua Saxe, Junteng Jia, Kalyan Vasuden Alwala, Karthik Prasad, Kartikeya Upasani, Kate Plawiak, Ke Li, Kenneth Heafield, Kevin Stone, Khalid El-Arini, Krithika Iyer, Kshitiz Malik, Kuenley Chiu, Kunal Bhalla, Kushal Lakhota, Lauren Rantala-Yearly, Laurens van der Maaten, Lawrence Chen, Liang Tan, Liz Jenkins, Louis Martin, Lovish Madaan, Lubo Malo, Lukas Blecher, Lukas Landzaat, Luke de Oliveira, Madeline Muzzi, Mahesh Pasupuleti, Mannat Singh, Manohar Paluri, Marcin Kardas, Maria Tsimpoukelli, Mathew Oldham, Mathieu Rita, Maya Pavlova, Melanie Kambadur, Mike Lewis, Min Si, Mitesh Kumar Singh, Mona Hassan, Naman Goyal, Narjes Torabi, Nikolay Bashlykov, Nikolay Bogoychev, Niladri Chatterji, Ning Zhang, Olivier Duchenne, Onur Çelebi, Patrick Alrassy, Pengchuan Zhang, Pengwei Li, Petar Vasic, Peter Weng, Prajjwal Bhargava, Pratik Dubal, Praveen Krishnan, Punit Singh Koura, Puxin Xu, Qing He, Qingxiao Dong, Ragavan Srinivasan, Raj Ganapathy, Ramon Calderer, Ricardo Silveira Cabral, Robert Stojnic, Roberta Raileanu, Rohan Maheswari, Rohit Girdhar, Rohit Patel, Romain Sauvestre, Ronnie Polidor, Roshan Sumbaly, Ross Taylor, Ruan Silva, Rui Hou, Rui Wang, Saghar Hosseini, Sahana Chennabasappa, Sanjay Singh, Sean Bell, Seohyun Sonia Kim, Sergey Edunov, Shaoliang Nie, Sharan Narang, Sharath Raparth, Sheng Shen, Shengye Wan, Shruti Bhosale, Shun Zhang, Simon Vandenhende, Soumya Batra, Spencer Whitman, Sten Sootla, Stephane Collot, Suchin Gururangan, Sydney Borodinsky, Tamar Herman, Tara Fowler, Tarek Sheasha, Thomas Georgiou, Thomas Scialom, Tobias Speckbacher, Todor Mihaylov, Tong Xiao, Ujjwal Karn, Vedanuj Goswami, Vibhor Gupta, Vignesh Ramanathan, Viktor Kerkez, Vincent Gonguet, Virginie Do, Vish Vogeti, Vitor Albiero, Vladan Petrovic, Weiwei Chu, Wenhan Xiong, Wenyin Fu, Whitney Meers, Xavier Martinet, Xiaodong Wang, Xiaofang Wang, Xiaoqing Ellen Tan, Xide Xia, Xinfeng Xie, Xuchao Jia, Xuewei Wang, Yaelle Goldschlag, Yashesh Gaur, Yasmine Babaei, Yi Wen, Yiwen Song, Yuchen Zhang, Yue Li, Yuning Mao, Zacharie Delpierre Coudert, Zheng Yan, Zhengxing Chen, Zoe Papakipos, Aaditya Singh, Aayushi Srivastava, Abha Jain, Adam Kelsey, Adam Shajnfeld, Adithya Gangidi, Adolfo Victoria, Ahuva Goldstand, Ajay Menon, Ajay Sharma, Alex Boesenberg, Alexei Baevski, Allie Feinstein, Amanda Kallet, Amit Sangani, Amos Teo, Anam Yunus, Andrei Lupu, Andres Alvarado, Andrew Caples, Andrew Gu, Andrew Ho, Andrew Poulton, Andrew Ryan, Ankit Ramchandani, Annie Dong, Annie Franco, Anuj Goyal, Aparajita Saraf, Arkabandhu Chowdhury, Ashley Gabriel, Ashwin Bharambe, Assaf Eisenman, Azadeh Yazdan, Beau James, Ben Maurer, Benjamin Leonhardi, Bernie Huang, Beth Loyd, Beto De Paola, Bhargavi Paranjape, Bing Liu, Bo Wu, Boyu Ni, Braden Hancock, Bram Wasti, Brandon Spence, Brani Stojkovic, Brian Gamido, Britt Montalvo, Carl Parker, Carly Burton, Catalina Mejia, Ce Liu, Changhan Wang, Changkyu Kim, Chao Zhou, Chester Hu, Ching-Hsiang Chu, Chris Cai, Chris Tindal, Christoph Feichtenhofer, Cynthia Gao, Damon Civin, Dana Beaty, Daniel Kreymer, Daniel Li, David Adkins, David Xu, Davide Testuggine, Delia David, Devi Parikh, Diana Liskovich, Didem Foss, Dingkang Wang, Duc Le, Dustin Holland, Edward Dowling, Eissa Jamil, Elaine Montgomery, Eleonora Presani, Emily Hahn, Emily Wood, Eric-Tuan Le, Erik Brinkman, Esteban Arcaute, Evan Dunbar, Evan Smothers, Fei Sun, Felix Kreuk, Feng Tian, Filippos Kokkinos, Firat Ozgenel, Francesco Caggioni, Frank Kanayet, Frank Seide, Gabriela Medina Florez, Gabriella Schwarz, Gada Badeer, Georgia Swee, Gil Halpern, Grant Herman, Grigory Sizov, Guangyi, Zhang, Guna Lakshminarayanan, Hakan Inan, Hamid Shojanazeri, Han Zou, Hannah Wang, Hanwen Zha, Haroun Habeeb, Harrison Rudolph, Helen Suk, Henry Aspegren, Hunter Goldman, Hongyuan Zhan, Ibrahim Damlaj, Igor Molybog, Igor Tufanov, Ilias Leontiadis, Irina-Elena Veliche, Itai Gat, Jake Weissman, James Geboski, James Kohli, Janice Lam, Japhet Asher, Jean-Baptiste Gaya, Jeff Marcus, Jeff Tang, Jennifer Chan, Jenny Zhen, Jeremy Reizenstein, Jeremy Teboul, Jessica Zhong, Jian Jin, Jingyi Yang, Joe Cummings, Jon Carvill, Jon Shepard, Jonathan McPhie, Jonathan Torres, Josh Ginsburg, Junjie Wang, Kai Wu, Kam Hou U, Karan Saxena, Kartikay Khandelwal, Katayoun Zand, Kathy Matosich, Kaushik Veeraraghavan, Kelly Michelena, Keqian Li, Kiran Jagadeesh, Kun Huang, Kunal Chawla, Kyle Huang, Lailin Chen, Lakshya Garg, Lavender A, Leandro Silva, Lee Bell, Lei Zhang, Liangpeng Guo, Licheng Yu, Liron Moshkovich, Luca Wehrstedt, Madian Khabsa, Manav Avalani, Manish Bhatt, Martynas Mankus, Matan Hasson,

Matthew Lennie, Matthias Reso, Maxim Groshev, Maxim Naumov, Maya Lathi, Meghan Keneally, Miao Liu, Michael L. Seltzer, Michal Valko, Michelle Restrepo, Mihir Patel, Mik Vyatskov, Mikayel Samvelyan, Mike Clark, Mike Macey, Mike Wang, Miquel Jubert Hermoso, Mo Metanat, Mohammad Rastegari, Munish Bansal, Nandhini Santhanam, Natascha Parks, Natasha White, Navyata Bawa, Nayan Singhal, Nick Egebo, Nicolas Usunier, Nikhil Mehta, Nikolay Pavlovich Laptev, Ning Dong, Norman Cheng, Oleg Chernoguz, Olivia Hart, Omkar Salpekar, Ozlem Kalinli, Parkin Kent, Parth Parekh, Paul Saab, Pavan Balaji, Pedro Rittner, Philip Bontrager, Pierre Roux, Piotr Dollar, Polina Zvyagina, Prashant Ratanchandani, Pritish Yuvraj, Qian Liang, Rachad Alao, Rachel Rodriguez, Rafi Ayub, Raghatham Murthy, Raghu Nayani, Rahul Mitra, Rangaprabhu Parthasarathy, Raymond Li, Rebekkah Hogan, Robin Battey, Rocky Wang, Russ Howes, Ruty Rinott, Sachin Mehta, Sachin Siby, Sai Jayesh Bondu, Samyak Datta, Sara Chugh, Sara Hunt, Sargun Dhillon, Sasha Sidorov, Satadru Pan, Saurabh Mahajan, Saurabh Verma, Seiji Yamamoto, Sharadh Ramaswamy, Shaun Lindsay, Shuang Feng, Shenghao Lin, Shengxin Cindy Zha, Shishir Patil, Shiva Shankar, Shuqiang Zhang, Shuqiang Zhang, Sinong Wang, Sneha Agarwal, Soji Sajuyigbe, Soumith Chintala, Stephanie Max, Stephen Chen, Steve Kehoe, Steve Satterfield, Sudarshan Govindaprasad, Sumit Gupta, Summer Deng, Sungmin Cho, Sunny Virk, Suraj Subramanian, Sy Choudhury, Sydney Goldman, Tal Remez, Tamar Glaser, Tamara Best, Thilo Koehler, Thomas Robinson, Tianhe Li, Tianjun Zhang, Tim Matthews, Timothy Chou, Tzook Shaked, Varun Vontimitta, Victoria Ajayi, Victoria Montanez, Vijai Mohan, Vinay Satish Kumar, Vishal Mangla, Vlad Ionescu, Vlad Poenaru, Vlad Tiberiu Mihailescu, Vladimir Ivanov, Wei Li, Wencheng Wang, Wenwen Jiang, Wes Bouaziz, Will Constable, Xiaocheng Tang, Xiaoqian Wu, Xiaolan Wang, Xilun Wu, Xinbo Gao, Yaniv Kleinman, Yanjun Chen, Ye Hu, Ye Jia, Ye Qi, Yenda Li, Yilin Zhang, Ying Zhang, Yossi Adi, Youngjin Nam, Yu, Wang, Yu Zhao, Yuchen Hao, Yundi Qian, Yunlu Li, Yuzi He, Zachary DeVito, Zef Rosnbrick, Zhaojun Wen, Zhenyu Yang, Zhiwei Zhao, and Zhiyu Ma. The llama 3 herd of models. *arXiv preprint arXiv: 2407.21783*, 2024.

Michael Hahn and Mark Rofin. Why are sensitive functions hard for transformers? In Lun-Wei Ku, Andre Martins, and Vivek Srikumar, editors, *Proceedings of the 62nd Annual Meeting of the Association for Computational Linguistics (Volume 1: Long Papers)*, pages 14973–15008, Bangkok, Thailand, August 2024. Association for Computational Linguistics. doi: 10.18653/v1/2024.acl-long.800. URL <https://aclanthology.org/2024.acl-long.800/>.

Shibo Hao, Sainbayar Sukhbaatar, Dijia Su, Xian Li, Zhiting Hu, Jason Weston, and Yuandong Tian. Training large language models to reason in a continuous latent space. *arXiv preprint arXiv:2412.06769*, 2024.

Kaiming He, Xiangyu Zhang, Shaoqing Ren, and Jian Sun. Deep residual learning for image recognition. *arXiv preprint arXiv: 1512.03385*, 2015.

Gao Huang, Zhuang Liu, Laurens van der Maaten, and Kilian Q. Weinberger. Densely connected convolutional networks, 2018. URL <https://arxiv.org/abs/1608.06993>.

Albert Q. Jiang, Alexandre Sablayrolles, Arthur Mensch, Chris Bamford, Devendra Singh Chaplot, Diego de las Casas, Florian Bressand, Gianna Lengyel, Guillaume Lample, Lucile Saulnier, Lélio Renard Lavaud, Marie-Anne Lachaux, Pierre Stock, Teven Le Scao, Thibaut Lavril, Thomas Wang, Timothée Lacroix, and William El Sayed. Mistral 7b. *arXiv preprint arXiv: 2310.06825*, 2023.

Guilherme Penedo, Hynek Kydlícek, Loubna Ben allal, Anton Lozhkov, Margaret Mitchell, Colin Raffel, Leandro Von Werra, and Thomas Wolf. The fineweb datasets: Decanting the web for the finest text data at scale, 2024. URL <https://arxiv.org/abs/2406.17557>.

Qwen, :, An Yang, Baosong Yang, Beichen Zhang, Binyuan Hui, Bo Zheng, Bowen Yu, Chengyuan Li, Dayiheng Liu, Fei Huang, Haoran Wei, Huan Lin, Jian Yang, Jianhong Tu, Jianwei Zhang, Jianxin Yang, Jiaxi Yang, Jingren Zhou, Junyang Lin, Kai Dang, Keming Lu, Keqin Bao, Kexin Yang, Le Yu, Mei Li, Mingfeng Xue, Pei Zhang, Qin Zhu, Rui Men, Runji Lin, Tianhao Li, Tingyu Xia, Xingzhang Ren, Xuancheng Ren, Yang Fan, Yang Su, Yichang Zhang, Yu Wan, Yuqiong Liu, Zeyu Cui, Zhenru Zhang, and Zihan Qiu. Qwen2.5 technical report. *arXiv preprint arXiv: 2412.15115*, 2024.

David Raposo, Sam Ritter, Blake Richards, Timothy Lillicrap, Peter Conway Humphreys, and Adam Santoro. Mixture-of-depths: Dynamically allocating compute in transformer-based language models, 2024. URL <https://arxiv.org/abs/2404.02258>.

Aarohi Srivastava, Abhinav Rastogi, Abhishek Rao, Abu Awal Md Shoeb, Abubakar Abid, Adam Fisch, Adam R. Brown, Adam Santoro, Aditya Gupta, Adrià Garriga-Alonso, Agnieszka Kluska, Aitor Lewkowycz, Akshat Agarwal, Alethea Power, Alex Ray, Alex Warstadt, Alexander W. Kocurek, Ali Safaya, Ali Tazarv, Alice Xiang, Alicia Parrish, Allen Nie, Aman Hussain, Amanda Askell, Amanda Dsouza, Ambrose Slone, Ameet Rahane, Anantharaman S. Iyer, Anders Andreassen, Andrea Madotto, Andrea Santilli, Andreas Stuhlmüller, Andrew M. Dai, Andrew La, Andrew K. Lampinen, Andy Zou, Angela Jiang, Angelica Chen, Anh Vuong, Animesh Gupta, Anna Gottardi, Antonio Norelli, Anu Venkatesh, Arash Gholamidavoodi, Arfa Tabassum, Arul Menezes, Arun Kirubarajan, Asher Mollokandov, Ashish Sabharwal, Austin Herrick, Avia Efrat, Aykut Erdem, Ayla Karakas, B. Ryan Roberts, Bao Sheng Loe, Barret Zoph, Bartłomiej Bojanowski, Batuhan Özürt, Behnam Hedayatnia, Behnam Neyshabur, Benjamin Inden, Benno Stein, Berk Ekmekci, Bill Yuchen Lin, Blake Howald, Bryan Orinion, Cameron Diao, Cameron Dour, Catherine Stinson, Cedrick Argueta, Cèsar Ferri Ramírez, Chandan Singh, Charles Rathkopf, Chenlin Meng, Chitta Baral, Chiyu Wu, Chris Callison-Burch, Chris Waites, Christian Voigt, Christopher D. Manning, Christopher Potts, Cindy Ramirez, Clara E. Rivera, Clemencia Siro, Colin Raffel, Courtney Ashcraft, Cristina Garbacea, Damien Sileo, Dan Garrette, Dan Hendrycks, Dan Kilman, Dan Roth, Daniel Freeman, Daniel Khashabi, Daniel Levy, Daniel Moseguí González, Danielle Perszyk, Danny Hernandez, Danqi Chen, Daphne Ippolito, Dar Gilboa, David Dohan, David Drakard, David Jurgens, Debajyoti Datta, Deep Ganguli, Denis Emelin, Denis Kleyko, Deniz Yuret, Derek Chen, Derek Tam, Dieuwke Hupkes, Diganta Misra, Dilyar Buzan, Dimitri Coelho Mollo, Diyi Yang, Dong-Ho Lee, Dylan Schrader, Ekaterina Shutova, Ekin Dogus Cubuk, Elad Segal, Eleanor Hagerman, Elizabeth Barnes, Elizabeth Donoway, Ellie Pavlick, Emanuele Rodolà, Emma Lam, Eric Chu, Eric Tang, Erkut Erdem, Ernie Chang, Ethan A. Chi, Ethan Dyer, Ethan J. Jerzak, Ethan Kim, Eunice Engefu Manyasi, Evgenii Zheltonozhskii, Fanyue Xia, Fatemeh Siar, Fernando Martínez-Plumed, Francesca Happé, François Chollet, Frieda Rong, Gaurav Mishra, Genta Indra Winata, Gerard de Melo, Germán Kruszewski, Giambattista Parascandolo, Giorgio Mariani, Gloria Wang, Gonzalo Jaimovich-López, Gregor Betz, Guy Gur-Ari, Hana Galijasevic, Hannah Kim, Hannah Rashkin, Hannaneh Hajishirzi, Harsh Mehta, Hayden Bogar, Henry Shevlin, Hinrich Schütze, Hiromu Yakura, Hongming Zhang, Hugh Mee Wong, Ian Ng, Isaac Noble, Jaap Jumelet, Jack Geissinger, Jackson Kernion, Jacob Hilton, Jaehoon Lee, Jaime Fernández Fisac, James B. Simon, James Koppel, James Zheng, James Zou, Jan Kocon, Jana Thompson, Janelle Wingfield, Jared Kaplan, Jarema Radom, Jascha Sohl-Dickstein, Jason Phang, Jason Wei, Jason Yosinski, Jekaterina Novikova, Jelle Bosscher, Jennifer Marsh, Jeremy Kim, Jeroen Taal, Jesse H. Engel, Jesujoba Alabi, Jiacheng Xu, Jiaming Song, Jillian Tang, Joan Waweru, John Burden, John Miller, John U. Balis, Jonathan Batchelder, Jonathan Berant, Jörg Frohberg, Jos Rozen, José Hernández-Orallo, Joseph Boudeman, Joseph Guerr, Joseph Jones, Joshua B. Tenenbaum, Joshua S. Rule, Joyce Chua, Kamil Kanclerz, Karen Livescu, Karl Krauth, Karthik Gopalakrishnan, Katerina Ignatyeva, Katja Markert, Kaustubh D. Dhole, Kevin Gimpel, Kevin Omondi, Kory W. Mathewson, Kristen Chiaffullo, Ksenia Shkaruta, Kumar Shridhar, Kyle McDonell, Kyle Richardson, Laria Reynolds, Leo Gao, Li Zhang, Liam Dugan, Lianhui Qin, Lidia Contreras Ochando, Louis-Philippe Morency, Luca Moschella, Lucas Lam, Lucy Noble, Ludwig Schmidt, Luheng He, Luis Oliveros Colón, Luke Metz, Lütfi Kerem Senel, Maarten Bosma, Maarten Sap, Maartje ter Hoeve, Maheen Farooqi, Manaal Faruqui, Mantas Mazeika, Marco Baturan, Marco Marelli, Marco Maru, María José Ramírez-Quintana, Marie Tolkiehn, Mario Giulianelli, Martha Lewis, Martin Potthast, Matthew L. Leavitt, Matthias Hagen, Mátyás Schubert, Medina Baitemirova, Melody Arnaud, Melvin McElrath, Michael A. Yee, Michael Cohen, Michael Gu, Michael I. Ivanitskiy, Michael Starritt, Michael Strube, Michal Swedrowski, Michele Bevilacqua, Michihiro Yasunaga, Mihir Kale, Mike Cain, Mimee Xu, Mirac Suzgun, Mitch Walker, Mo Tiwari, Mohit Bansal, Moin Aminnaseri, Mor Geva, Mozhdeh Gheini, Mukund Varma T., Nanyun Peng, Nathan A. Chi, Nayeon Lee, Neta Gur-Ari Krakover, Nicholas Cameron, Nicholas Roberts, Nick Doiron, Nicole Martinez, Nikita Nangia, Niklas Deckers, Niklas Muennighoff, Nitish Shirish Keskar, Niveditha Iyer, Noah Constant, Noah Fiedel, Nuan Wen, Oliver Zhang, Omar Agha, Omar Elbaghdadi, Omer Levy, Owain Evans, Pablo Antonio Moreno Casares, Parth Doshi, Pascale Fung, Paul Pu Liang, Paul Vicol, Pegah Alipoormolabashi, Peiyuan Liao, Percy Liang, Peter Chang, Peter Eckersley, Phu Mon Htut, Pinyu Hwang, Piotr Milkowski, Piyush Patil, Pouya Pezeshkpour,

Priti Oli, Qiaozhu Mei, Qing Lyu, Qinlang Chen, Rabin Banjade, Rachel Etta Rudolph, Raefer Gabriel, Rahel Habacker, Ramon Risco, Raphaël Millière, Rhythm Garg, Richard Barnes, Rif A. Saurous, Riku Arakawa, Robbe Raymaekers, Robert Frank, Rohan Sikand, Roman Novak, Roman Sitelew, Ronan LeBras, Rosanne Liu, Rowan Jacobs, Rui Zhang, Ruslan Salakhutdinov, Ryan Chi, Ryan Lee, Ryan Stovall, Ryan Teehan, Rylan Yang, Sahib Singh, Saif M. Mohammad, Sajant Anand, Sam Dillavou, Sam Shleifer, Sam Wiseman, Samuel Gruetter, Samuel R. Bowman, Samuel S. Schoenholz, Sanghyun Han, Sanjeev Kwatra, Sarah A. Rous, Sarik Ghazarian, Sayan Ghosh, Sean Casey, Sebastian Bischoff, Sebastian Gehrmann, Sebastian Schuster, Sepideh Sadeghi, Shadi Hamdan, Sharon Zhou, Shashank Srivastava, Sherry Shi, Shikhar Singh, Shima Asaadi, Shixiang Shane Gu, Shubh Pachchigar, Shubham Toshniwal, Shyam Upadhyay, Shyamolima (Shammie) Debnath, Siamak Shakeri, Simon Thormeyer, Simone Melzi, Siva Reddy, Sneha Priscilla Makini, Soo-Hwan Lee, Spencer Torene, Sriharsha Hatwar, Stanislav Dehaene, Stefan Divic, Stefano Ermon, Stella Biderman, Stephanie Lin, Stephen Prasad, Steven T. Piantadosi, Stuart M. Shieber, Summer Mishnergh, Svetlana Kiritchenko, Swaroop Mishra, Tal Linzen, Tal Schuster, Tao Li, Tao Yu, Tariq Ali, Tatsu Hashimoto, Te-Lin Wu, Théo Desbordes, Theodore Rothschild, Thomas Phan, Tianle Wang, Tiberius Nkinyili, Timo Schick, Timofei Kornev, Titus Tunduny, Tobias Gerstenberg, Trenton Chang, Trishala Neeraj, Tushar Khot, Tyler Shultz, Uri Shaham, Vedant Misra, Vera Demberg, Victoria Nyamai, Vikas Raunak, Vinay V. Ramasesh, Vinay Uday Prabhu, Vishakh Padmakumar, Vivek Srikanth, William Fedus, William Saunders, William Zhang, Wout Vossen, Xiang Ren, Xiaoyu Tong, Xinran Zhao, Xinyi Wu, Xudong Shen, Yadollah Yaghoobzadeh, Yair Laikez, Yangqiu Song, Yasaman Bahri, Yejin Choi, Yichi Yang, Yiding Hao, Yifu Chen, Yonatan Belinkov, Yu Hou, Yufang Hou, Yuntao Bai, Zachary Seid, Zhuoye Zhao, Zijian Wang, Zijie J. Wang, Zirui Wang, and Ziyi Wu. Beyond the imitation game: Quantifying and extrapolating the capabilities of language models. *Trans. Mach. Learn. Res.*, 2023, 2023. URL <https://openreview.net/forum?id=uyTL5Bvosj>.

Rupesh Kumar Srivastava, Klaus Greff, and Jürgen Schmidhuber. Highway networks. *arXiv preprint arXiv: 1505.00387*, 2015.

Ian Tenney, Dipanjan Das, and Ellie Pavlick. BERT rediscovers the classical NLP pipeline. In Anna Korhonen, David Traum, and Lluís Márquez, editors, *Proceedings of the 57th Annual Meeting of the Association for Computational Linguistics*, pages 4593–4601, Florence, Italy, July 2019. Association for Computational Linguistics. doi: 10.18653/v1/P19-1452. URL <https://aclanthology.org/P19-1452/>.

Ashish Vaswani, Noam Shazeer, Niki Parmar, Jakob Uszkoreit, Llion Jones, Aidan N. Gomez, Łukasz Kaiser, and Illia Polosukhin. Attention is all you need. *NEURIPS*, 2017.

Elena Voita, Rico Sennrich, and Ivan Titov. The bottom-up evolution of representations in the transformer: A study with machine translation and language modeling objectives. In Kentaro Inui, Jing Jiang, Vincent Ng, and Xiaojun Wan, editors, *Proceedings of the 2019 Conference on Empirical Methods in Natural Language Processing and the 9th International Joint Conference on Natural Language Processing (EMNLP-IJCNLP)*, pages 4396–4406, Hong Kong, China, November 2019. Association for Computational Linguistics. doi: 10.18653/v1/D19-1448. URL <https://aclanthology.org/D19-1448/>.

Alex Wang, Amanpreet Singh, Julian Michael, Felix Hill, Omer Levy, and Samuel R. Bowman. Glue: A multi-task benchmark and analysis platform for natural language understanding. *Ws*, 2018.

Alex Wang, Yada Pruksachatkun, Nikita Nangia, Amanpreet Singh, Julian Michael, Felix Hill, Omer Levy, and Samuel R. Bowman. SuperGlue: A stickier benchmark for general-purpose language understanding systems. *Neural Information Processing Systems*, 2019.

Jason Wei, Xuezhi Wang, Dale Schuurmans, Maarten Bosma, Brian Ichter, Fei Xia, Ed H. Chi, Quoc V. Le, and Denny Zhou. Chain-of-thought prompting elicits reasoning in large language models. *Advances in Neural Information Processing Systems*, 35:24824–24837, 2022.

Xixin Wu, Hui Lu, Kun Li, Zhiyong Wu, Xunying Liu, and Helen Meng. Hiformer: Sequence modeling networks with hierarchical attention mechanisms. *IEEE/ACM Transactions on Audio, Speech, and Language Processing*, 31:3993–4003, 2023. doi: 10.1109/TASLP.2023.3313428. URL <https://doi.org/10.1109/TASLP.2023.3313428>.

Defa Zhu, Hongzhi Huang, Zihao Huang, Yutao Zeng, Yunyao Mao, Banggu Wu, Qiyang Min, and Xun Zhou. Hyper-connections. *arXiv preprint arXiv: 2409.19606*, 2024.

A Experimental Setup Details

Language Modeling. We observe that omitting weight decay on the LIME router weights enjoys better performance and setting the router’s learning rate to 1×10^{-2} boosts model performance by speeding up router convergence and circuit formation. To preserve the standard Transformer’s information flow at the start of the training, we initialize the slice $R_{\ell,h',h}^{(\ell)} = \delta_{h',h}$ (identity across heads). Other coefficients are initialized randomly via Kaiming uniform to stabilize mixtures at the start of the training. Random initialization of all weights resulted in worse overall model performance. Hyperparameter values are summarized in Table 2, and the detailed model architecture is given in Table 3. Additional training loss visualizations are available in Figure 11 for full attention and in Figure 10 for Grouped Query Attention.

We used NVIDIA H100 GPUs and spent about 2400 GPU-days on all experiments including preliminary research.

ProsQA Fine-Tuning. We fine-tune pretrained LLaMa 150M and LIME 150M on approximately 18,000 sequences for 10 epochs. We use learning rate of 1×10^{-4} with linear decay and warmup during the first epoch, effective batch size is 128. Trained models are then evaluated on the test subset via open generation of reasoning steps and answers.

Arithmetic Expression Task. We train models and evaluate them on open-ended generation of solutions given initial expression, from which we extract the answers and calculate accuracy on the test subset. We train 4-layer models (with 4 attention heads and model dim is 32) on datasets with 50,000 samples per each number of operands for 200 epochs. Learning rate is 1×10^{-3} with linear decay.

Hyperparameter	Value
Optimizer	AdamW
Learning Rate	0.001
LIME Router Learning Rate	0.01
Weight Decay	0.1
β_1	0.9
β_2	0.95
ϵ	1×10^{-8}
Scheduler	cosine
Warmup Steps	200
Min LR	1×10^{-6}
Mixed Precision	bf16
Gradient Clipping	1.0
Sequence Length	2048
Batch Size	1024
Training Steps	20,000

Table 2: Key training hyperparameters used in experiments.

Parameter	Value
Vocab Size	50,257
Hidden Size	2048
Intermediate Size	8192
Number of Hidden Layers	16
Number of Attention Heads	32
Number of Key-Value Heads	8 (GQA) and 32 (otherwise)
Tie Word Embeddings	True

Table 3: Base model architecture at 1B scale.

B Synthetic Benchmarks

ProsQA

Question: "Every shumpus is a rempus. Every shumpus is a yimpus. Every terpus is a fompus. Every terpus is a gerpus. Every gerpus is a brimpus. Alex is a rempus. Every rorpus is a scrompus. Every rorpus is a yimpus. Every terpus is a brimpus. Every brimpus is a lempus. Tom is a terpus. Every shumpus is a timpus. Every yimpus is a boompus. Davis is a shumpus. Every gerpus is a lorpus. Davis is a fompus. Every shumpus is a boompus. Every shumpus is a rorpus. Every terpus is a lorpus. Every boompus is a timpus. Every fompus is a yerpus. Tom is a dumpus. Every rempus is a rorpus. Is Tom a lempus or scrompus?"

Steps: "Tom is a terpus. Every terpus is a brimpus. Every brimpus is a lempus."

Answer: "Tom is a lempus."

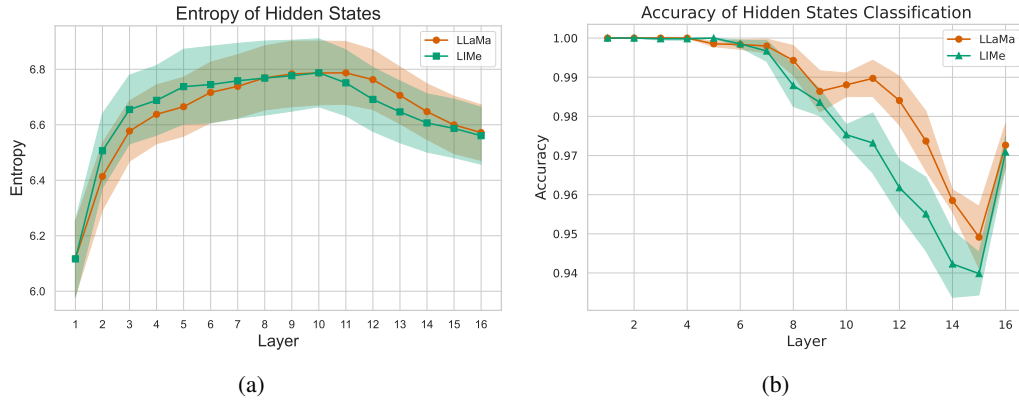
Arithmetic Expression Task

Input:

$$(7 + 5) \div (6 + 4 \times 3 - 2 \times 7) =$$

Output:

$$\begin{aligned} 12 \div (6 + 4 \times 3 - 2 \times 7) &= 12 \div (6 + 12 - 2 \times 7) \\ &= 12 \div (18 - 2 \times 7) \\ &= 12 \div (18 - 14) \\ &= 12 \div 4 \\ &= 3 \end{aligned}$$

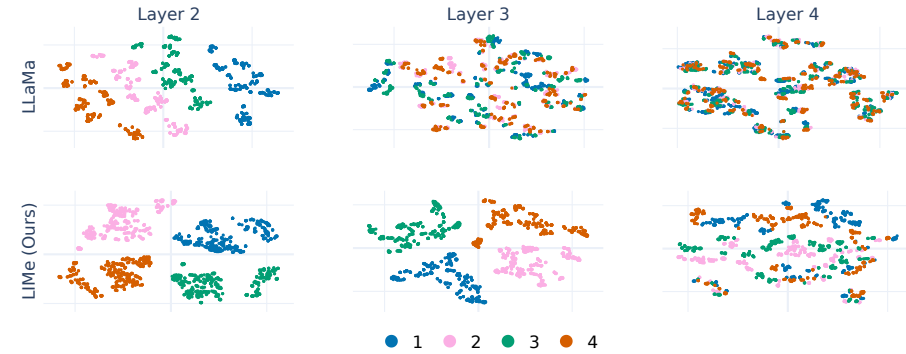


(a)

(b)

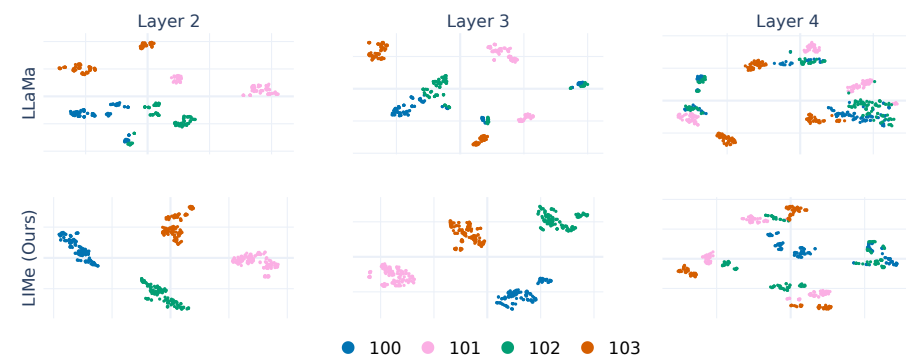
Figure 7: (a) Matrix entropy of the hidden states across layers on the FineWeb Edu subset. We do not observe a significant difference between LIME and LLaMa in this experiment. (b) Classification accuracy of the hidden states, with standard deviation, measured over five cross-validation folds. Because the hidden states in LIME do not need to store all the information in the residual stream, they become less separable. See Section 5.2 for more details.

Values Representations



(a)

Values Representations



(b)

Figure 8: t-SNE of close numbers' values representations of models trained on Arithmetic Expressions Task. (a) For 1, 2, 3, 4. (b) For 100, 101, 102, 103. See Section 5.3.2.

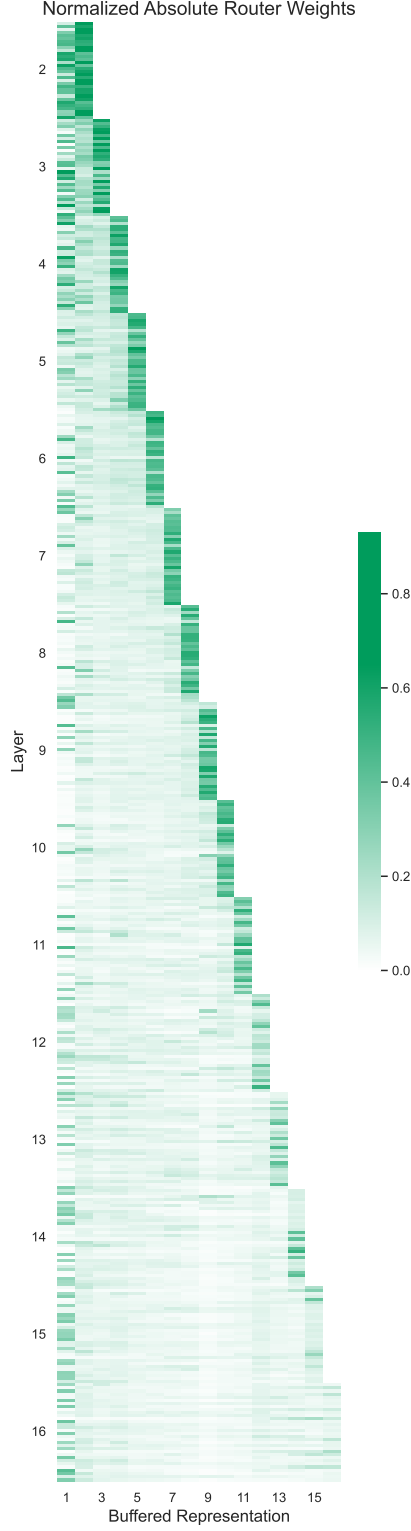


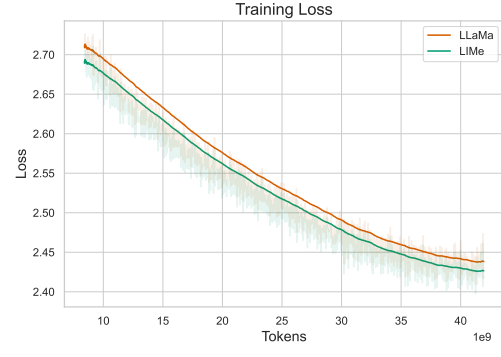
Figure 9: Magnitudes of router weights averaged among buffered heads and normalized among buffered layers. Each cell represents ratio of attention for each buffered representation in the specific head.



Figure 10: Training loss per tokens trained on for LLaMa and LiMe with GQA. It shows that LiMe is more data efficient. See Section 5.1 for more details.



(a)



(b)

Figure 11: Training loss for LLaMa and LiMe without GQA. (a) shows that LiMe has a substantially lower loss with a similar amount of FLOPs. (b) shows that LiMe is more data efficient. See Section 5.1 for more details.

C Additional Benchmarks

Model	COPA	MultiRC	WiC	QNLI	WNLI	Avg
LLaMA	75.80	43.24	50.00	49.49	51.27	53.96
HC	74.00	54.34	49.72	49.43	56.34	56.77
LIMe	75.20	56.15	50.44	51.43	56.06	57.86

Table 4: GLUE and SuperGLUE benchmarks accuracies (%) on 1B GQA models (3-shot), with average over the five tasks.

Model	ARC-E	ARC-C	HellaSwag	OBQA	Avg
LLaMA	70.45	38.70	52.55	37.68	49.85
HC	71.15	37.63	54.04	40.08	50.73
LIMe	71.15	39.30	52.85	39.68	50.75

Table 5: QA benchmarks accuracies (%) on 1B GQA models (3-shot), with average over the four tasks.

Model	KV	Induction	DisambQA	LD-5	LD-3	IR	CO	Avg
LLaMA	45.94	54.20	30.16	19.44	33.60	12.94	16.97	30.46
HC	51.68	51.59	26.20	19.92	33.87	15.29	18.48	31.00
LIMe	55.64	55.36	30.23	20.72	34.47	14.82	17.39	32.66

Table 6: Accuracies (%) of 3-shot 1B GQA models on BIG-Bench tasks: Key–Value Maps (KV), Mathematical Induction, Disambiguation QA, Logical Deduction for 3 and 5 objects (LD-3, LD-5), Implicit Relations (IR), and Reasoning About Colored Objects (CO).

D Router Ablation

We conduct an ablation study to assess the importance of learning full per-layer, per-head router weights in LIMe. Specifically, we compare the standard LIMe routing against several constrained variants on the 150M-parameter model, evaluating their impact on perplexity:

- **Fixed Average (average):** Aggregates all buffered Key–Value representations via a uniform average, without any learned head-specific weighting.
- **Recent- j (last- j):** Restricts each layer ℓ to attend only to the most recent $\min(\ell, j)$ buffered representations; router weights for these representations are learned.
- **Initial- j (first- j):** Restricts each layer ℓ to attend only to the first $\min(\ell, j)$ buffers plus the immediately preceding layer; router weights for these are learned.

Model	Perplexity	Change to LIME
LLaMA	16.4611	+3.36%
LIME average	16.4611	+3.36%
LIME last-2	16.2810	+2.22%
LIME last-4	16.1675	+1.51%
LIME last-6	16.1351	+1.31%
LIME first-2	15.9746	+0.30%
LIME first-4	15.9586	+0.20%
LIME first-6	15.9906	+0.40%
LIME	15.9267	—

Table 7: Impact of constrained routing schemes on validation perplexity for the 150M-parameter model. Table reports perplexity for each scheme and the relative change with respect to the full LIME model. The average variant fails to improve over the LLaMA baseline, indicating that uniform pooling of past representations is insufficient. Constraining attention to fixed windows of layers (last- j and first- j) yields modest gains but still underperforms the unrestricted router. By contrast, the full LIME routing achieves the lowest perplexity (15.9267), corresponding to a 3.36% reduction relative to LLaMA, thereby confirming the necessity of learning full, per-head, per-layer router weights for optimal performance.

E LIME Pseudocode

```

1  class LIMERouter(nn.Module):
2      def __init__(self, config, layer_idx):
3          super().__init__()
4          bound = math.sqrt(
5              3 / (layer_idx + 1) * config.num_kv_heads
6          )
7          weights = torch.empty(
8              config.num_kv_heads,
9              (layer_idx + 1) * config.num_kv_heads,
10             ).uniform_(-bound, bound)
11         weights[:, -config.num_kv_heads:] = torch.eye(
12             config.num_kv_heads
13         )
14         self.weights = nn.Parameter(weights)
15
16     def forward(self, kv_buffer):
17         # kv_buffer shape = [(layer_idx + 1) * kv_h, 2 * b * t * hd]
18         return self.weights.mm(kv_buffer)
19
20
21 class LIMEAttention(LlamaAttention):
22     def __init__(self, config, layer_idx):
23         super().__init__(config, layer_idx)
24         if layer_idx > 0:
25             self.lime_router = LIMERouter(config, layer_idx)
26
27     def forward(self, hidden_states, kv_buffer):
28         query_states = self.q_proj(hidden_states).reshape(b, h, t, hd)
29         key_states = self.k_proj(hidden_states).reshape(b, kv_h, t, hd)
30         value_states = self.v_proj(hidden_states).reshape(b, kv_h, t, hd)
31         kv_buffer.add_(key_states, value_states)
32         if self.layer_idx > 0:
33             key_states, value_states = self.lime_router(kv_buffer)
34             attn_output = scaled_dot_product_attention(
35                 query_states, key_states, value_states
36             )
37             attn_output = self.o_proj(
38                 attn_output.transpose(1, 2).reshape(b, t, -1)
39             )

```

```

40         return attn_output, kv_buffer
41
42
43 class LIMELayer(LlamaDecoderLayer):
44     def __init__(self, config, layer_idx):
45         super().__init__(config, layer_idx)
46         self.self_attn = LIMEAttention(config, layer_idx)
47
48     def forward(self, hidden_states, kv_buffer):
49         residual = hidden_states
50         hidden_states = self.input_layernorm(hidden_states)
51         attn_out, kv_buffer = self.self_attn(hidden_states, kv_buffer)
52         hidden_states = residual + attn_out
53
54         residual = hidden_states
55         hidden_states = self.post_attention_layernorm(hidden_states)
56         hidden_states = self.mlp(hidden_states)
57         hidden_states = residual + hidden_states
58
59     return hidden_states, kv_buffer
60
61
62 class LIMEModel(LlamaModel):
63     def __init__(self, config):
64         super().__init__(config)
65         self.layers = [
66             LIMELayer(config, i) for i in range(config.num_hidden_layers)
67         ]
68
69     def forward(self, input_ids):
70         hidden_states = self.embed_tokens(input_ids)
71         kv_buffer = init_kv_buffer()
72         for layer in self.layers:
73             hidden_states, kv_buffer = layer(hidden_states, kv_buffer)
74         return hidden_states

```

F Efficiency

MHA	Model	# Parameters (B)	FLOPs (T)
GQA	LLaMa	1.07607	2.7615
	LIME	1.07608 (+0.00%)	2.7638 (+0.08%)
	HC	1.07640 (+0.03%)	2.7701 (+0.31%)
Full	LLaMa	1.17674	2.9679
	LIME	1.17687 (+0.01%)	3.0041 (+1.22%)
	HC	1.17706 (+0.03%)	2.9764 (+0.29%)

Table 8: Model size (# parameters, in billions) and forward FLOPs for LIME and Hyper-connections (HC) relative to LLaMa under grouped-query attention (GQA) and full attention. We used `torch.jit.trace` to record all operations and estimated FLOPs via the `fvcore` library, based on tensor shapes and ATen operators. Total training FLOPs are approximated as $3 \times$ forward FLOPs, accounting for both forward and backward passes [Anthony et al., 2023].

MHA	RO	Model	Step Time (ms)	Train Peak Memory (GB)
GQA	+	LLaMa	65.770	16.035
		LIME	66.533 (+1.16%)	16.035 (+0.00%)
		HC	81.003 (+23.16%)	16.040 (+0.03%)
	-	LLaMa	66.404	20.489
		LIME	67.449 (+1.57%)	20.490 (+0.00%)
		HC	83.265 (+25.39%)	21.693 (+5.88%)
Full	+	LLaMa	69.776	17.535
		LIME	77.093 (+10.49%)	17.537 (+0.01%)
		HC	84.990 (+21.80%)	17.540 (+0.03%)
	-	LLaMa	70.258	22.364
		LIME	77.607 (+10.46%)	22.367 (+0.01%)
		HC	86.314 (+22.85%)	23.007 (+2.87%)

Table 9: Per-step latency and peak GPU memory usage of LIME and Hyper-connections (HC) in comparison to LLaMa under grouped-query attention (GQA) and full attention (Full), measured with PyTorch Inductor in default (–) and reduced-overhead (+) modes. LIME incurs only minimal overhead—effectively negligible in reduce-overhead mode—whereas HC exhibits substantially higher increases in both time and memory.

G LIME Visualisation

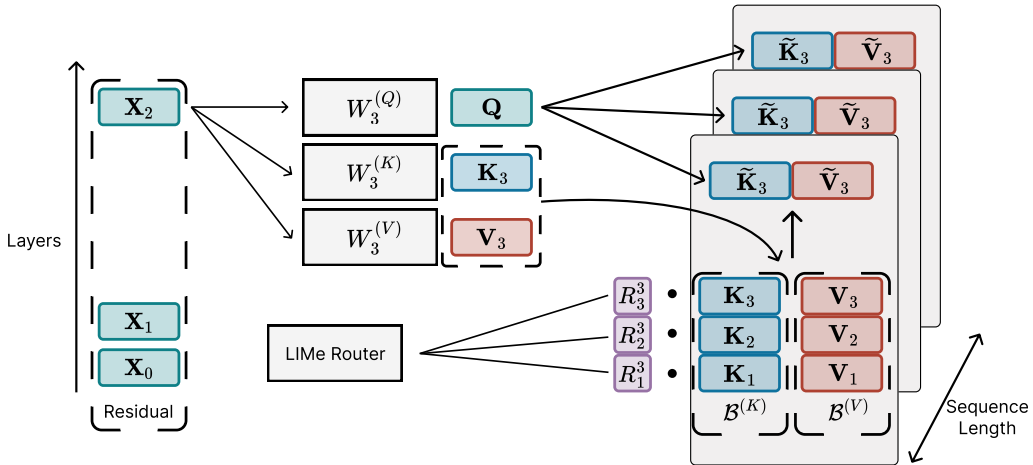


Figure 12: LIME routing scheme.